Acoustic Hydrogen Sensor

Zack Michaels, Spencer Perkins, William Schjelderup, Tessa Zolezzi

Project Sponsor: Mike Sexsmith

Project 2008
ENPH 459
Engineering Physics Project Laboratory
The University of British Columbia
April 8, 2020

Executive Summary

Hydrogen fuel cells purge the fuel line to get rid of contaminants that enter the system. This is done at a set time interval as an open loop control system. This excess purging of the fuel line leads to reduced fuel efficiency and cell lifespan. By adapting to a closed loop system, it is theorized that the efficiency can increase by up to 3% and improve the system's lifespan. Mike Sexsmith, CEO of OverDrive Fuel Cell Engineering (OverdriveFCE), requested a proof of concept that validated that an acoustic sensor is able to determine the concentration of hydrogen gas within a gas mixture. With this sensor, a closed loop control system could be successfully implemented with ±1% accuracy.

The capstone team designed, assembled, and implemented a prototype test bench to test the ability of ultrasonic sensors to measure the percent of helium (an inert substitute for hydrogen) in a gas mixture. Multiple tests were conducted to ensure that the test chamber and sensors were operating as expected. During initial trials, the team observed that the voltage output by the ultrasonic sensor decreased as the percent of helium increased. This observation was the first step in proving that ultrasonic sensors are able to detect changes in hydrogen percentages in gas mixtures. However, due to COVID-19 shutdowns, the team was not able to continue the project, which included running formal experiments.

Based on the initial observations, the team recommends to continue the project and run formal experiments while making a few changes to the test bench to improve performance. By collecting more data, a future team will be able to confirm that an ultrasonic sensor is able to measure the percent of hydrogen within a gas mixture with ±1% or better accuracy.

Table of Contents

Executive Summary **1**

Table of Contents **2**

Introduction **1**

Scope & Limitations 2

Discussion **4**

Theory 4

Fuel Cell Basics 4

Speed of Sound Calculations 5

Sensor Specifications 7

Sensitivity Analysis 9

Error Analysis 10

Design, approach, method, etc. 11

Tests, results, and discussion of results 14

Conclusions **15**

Recommendations **16**

Deliverables **17**

Appendices **1**

Appendix A: Technical Resources 1

Appendix B: Acoustic energy loss through medium boundaries 2

Appendix C: Deriving Voltage in term of Composition 3

Appendix D: Deriving Minimum Vessel Lengths 5

Appendix E: Numerical Error Analysis 6

Appendix F: Experimental Procedure 7

Appendix G: Bill of Materials 8

Appendix H: User Manuals 12

References **18**

Introduction

The sponsor for this project is Mike Sexsmith, CEO of OverdriveFCE in Burnaby, BC and a UBC Engineering Physics alumni. Mr. Sexsmith is sponsoring this project in order to increase the lifespan and efficiency of the fuel cells that OverdriveFCE designs and manufactures.

Mr. Sexsmith worked on a patent several years ago which described the use of an ultrasonic sensor to determine the concentration of hydrogen gas within an unknown gas mixture. If this project is able to show that one can use an ultrasonic sensor to determine the percent of hydrogen within a given accuracy, Mr. Sexsmith will buy the patent to further develop it. The sensor would then be installed within fuel cells to help determine the optimal time to flush the system based on the amount of hydrogen left in it. This is theorized to be up to 3% more fuel efficient (per fuel cell) than the current method.

The idea of using an acoustic sensor to detect properties of gases is a well-researched area with numerous patents, experiments, and industrial uses. For example, acoustic sensors are frequently used in industry to determine the quality of natural gas, which is important for maintaining optimal gas performance[1]. Ultrasonic sensors are also used to detect minute changes in the speed of sound from temperature variations to create a highly efficient thermometer[2]. This project differs as it focuses solely on finding the concentration of hydrogen gas under varying ambient conditions.

Currently, fuel cells operate under open-loop control by purging the fuel line at a set time interval. It is ideal to introduce feedback control into the system to increase its efficiency and lifespan. The feedback system determines the percent of hydrogen gas in the anode so that the system is able to purge at optimal times. This results in less fuel lost and prevents contaminants from binding to the reaction catalysts within the cell.

The goal of the project is to determine and verify if an ultrasonic transducer is able to find the hydrogen gas concentration within a ±1% range of the actual gas mixture composition. The transducer needs to be able to determine the concentration in pressure and temperature ranges of 1-3.5 bar and 20-65°C, respectively.

Scope & Limitations

This project was designed to answer the question: can the concentration of hydrogen be measured using the acoustic properties of a gas mixture at normal operating conditions? This meant testing a representative sample of mixtures of hydrogen and nitrogen with the concentration of hydrogen ranging from 50-100%. Due to the reactivity of hydrogen, it was decided to substitute hydrogen with helium as both gases have similar characteristics. Additionally, trace amounts of other gases are present within a fuel cell. However, these do not affect the acoustic properties greatly and are therefore left out from the project.

The sensor needs to provide an accurate measurement of helium content under a range of operating conditions that the fuel cell stack sees (1-3.5 bar absolute and 45-90°C). However, Mr. Sexsmith had advised that room temperature to approximately 65°C provides a reasonable range for testing. There are situations in which temperatures will fall outside of the normal operating range, dropping to as low as -40°C during a cold start. It was determined that testing the sensor in such extreme cases is nonessential at this baseline.

Furthermore, the accuracy of the sensor is paramount to its practicality. Through conversations with Mr. Sexsmith and calculations of the speed of sound in a given gas mixture, it was deemed essential to be accurate within 1% of the mixure's true composition. This had to be verifiable by standardized procedures. Initial designs relied on the theory of partial pressures or the use of mass flow meters to obtain a known gas mixture. These ideas replaced an unproven measurement technique with another. Ultimately, it was decided to roughly mix gases and then determine the true composition using a mass spectrometer.

The final major challenge was the placement of the transducer within the test chamber. Initial discussions made it clear that it is preferable to mount the sensor on the outside of the test chamber, as this would eliminate the need for the sponsor to alter the fuel cell itself. However, passing an acoustic signal through many solid-gas interfaces results in a near-total loss of the signal (Appendix B). Therefore, it was decided to validate the functionality of the system with the transducer secured inside the test chamber.

While the design and validation of an acoustic sensor was the goal of the project, a significant portion of the resources were used to develop the prototype test bench. This test bench was capable of providing the conditions needed to validate the sensor for each of the specifications described above, as well as be safe under pressure and vacuum. The test chamber was also designed to be hermetically sealed and the team observed minimal leak rate values. This allowed the system to hold a steady pressure and prevent contaminants from entering the system.

Discussion

Theory

Fuel Cell Basics

OverdriveFCE uses a proton exchange membrane (PEM) hydrogen fuel cell. PEM fuel cells convert chemical to electrical energy by catalytically splitting the H_2 molecules on the anode side into protons (H^+) and electrons (e^-). The protons pass through the electrolyte membrane to the cathode while the electrons move through a conductor to the cathode creating a voltage difference of ~0.7V per cell[3]. On the cathode side, the oxygen within air reacts with the protons and electrons to form water (H_2O) as a byproduct. This process can be seen in figure 1. Several of such cells are then connected together in parallel to form the fuel cell stack as seen in figure 2. The process mentioned above is governed by the chemical equations:

$$Anode : H_2 \rightarrow 2H^+ + 2e^-$$
$$Cathode : \frac{1}{2} + 2H^+ + 2e^- \rightarrow H_2O$$

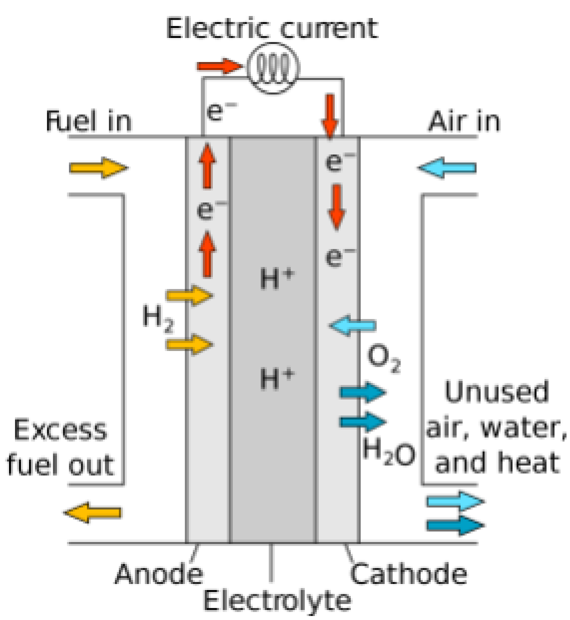

Figure 1. Fuel Cell Reaction[8]

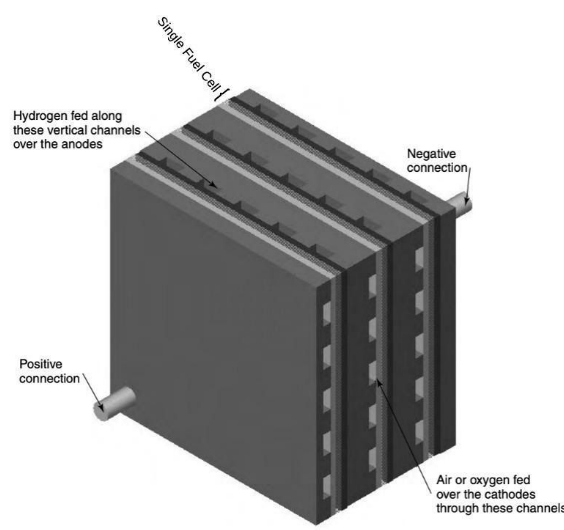

Figure 2. Fuel Cell CAD Diagram[3]

As the fuel cell runs it accumulates inert gases that must be purged. The typical gas percentages found within the fuel cell are 50-100% H_2, 0-30% $H_2O_{(g)}$ and the rest N_2, with trace amounts of particulate contaminants such as CO and CO_2. Ideally, the purge should occur when there are low concentrations of hydrogen to minimize hydrogen loss. However, there is currently no implemented way to detect the concentration of H_2 in the gas mixture within the fuel cell, but it is theoretically possible to do so by using the acoustic properties of the gases.

Speed of Sound Calculations

As the composition of a gas mixture changes, the speed of sound in that composition also changes. By modeling this phenomena, the amount of hydrogen within a fuel cell can be determined.

The speed of sound in an ideal gas is given by $v = \sqrt{\frac{\gamma RT}{M}}$ where γ is the gases adiabatic constant, R is molar gas constant, T is the absolute temperature and M is the gas molar weight in kg/mol. Notice that there is no functional dependence on pressure, this is because in an ideal gas the pressure and density both contribute to the speed of sound in such a way that the pressure cancels out[4]. Based on the aforementioned operating conditions, the gases are considered as ideal since any real gas can is approximately ideal at high absolute temperatures and low pressures[5]. Hydrogen, helium, and nitrogen gas are also non-polar molecules, further improving this approximation. Using the above equation, the speed of sound in gases vs. temperature is shown in the plot below. Helium is also included as it is used for prototyping as an alternative to hydrogen for safety purposes.

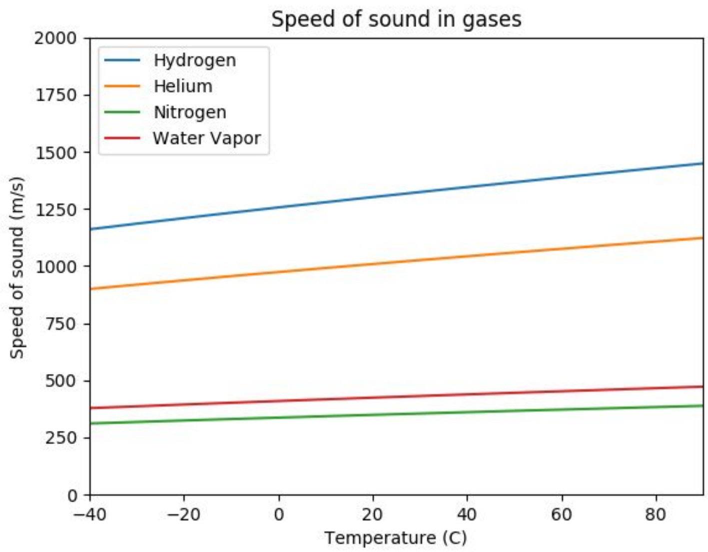

Figure 3: Speed of sound as a function of temperature for various gases

The plot shows that helium is a good substitute for hydrogen in prototyping because the speed of sound of hydrogen and helium are significantly larger than the speed of sound of the other gases. If this were not the case, it would not be possible to determine the concentrations of hydrogen solely based on the acoustic properties of a gas mixture. The water vapor within the mixture was neglected for the proof of concept.

The classical speed of sound in a mixture of ideal gases is described by the following equation[6].

$$v^2 = RT \frac{\sum x_i C_{pi}}{\sum x_i M_i \sum x_i (C_{pi} - R)} \quad (1)$$

Here x_i is the mole fraction of the ith element, and C_{pi} is the molar specific heat capacity at constant pressure of the ith element M_i is the molar mass of the ith element and R and T are the molar gas constant and absolute temperature respectively.

The specific heat capacity at constant pressure is defined (in SI units) as the quantity of heat required to raise the temperature of 1kg of gas by 1K (or equivalently 1 °C) at constant pressure. This quantity is a function of temperature only, but for ideal monatomic, diatomic and triatomic gases (the ones found within the fuel cell) it can be considered constant within the operating temperature range of the fuel cell[7].

The plot below shows the speed of sound v as a function of temperature T for common gas mixtures, using both H_2 (end goal) and He (prototyping) produced using equation 1. These graphs show the correlation between the percent mole fractions of the gases and the speed of sound, and how this changes at different temperatures. Thus, from the speed of sound and the temperature as inputs, the percent concentration of hydrogen can be determined. The plots show an increasing rate of change in speed of sound as the concentration of He or H_2 increases.

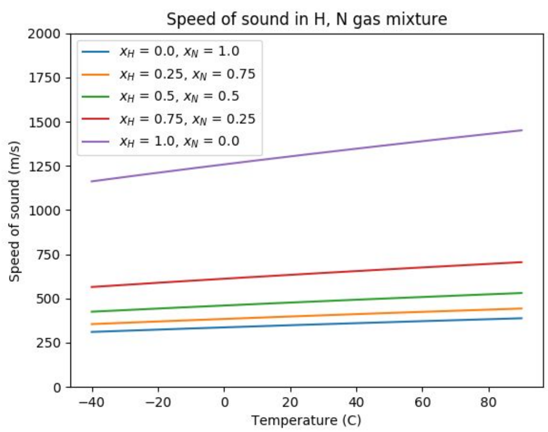

Figure 4a: Speed of sound variation with temperature for Hydrogen gas mixtures

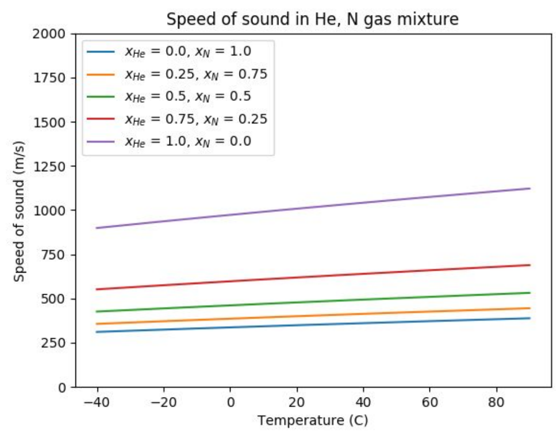

Figure 4b: Speed of sound variation with temperature for Helium gas mixtures

Sensor Specifications

A IFM UGT508 ultrasonic sensor was mounted via a through-hole at one end of the test chamber. The sensor works by sending out a sound pulse and receiving its echo off an object. The sensor then gives a voltage reading that varies linearly with the time of flight of the pulse. By using the sensor's teach mode, the distance bounds were set to give a reading of 10V when reading the time of flight in the vessel full of air. As helium gets pumped into the vessel the speed of sound increases, decreasing the time of flight and decreasing the voltage reading received by the sensor.

This sensor has a blind zone from 0 to 80 mm in air where it will display non-deterministic values. At 80 mm, it will display 0 volts and the voltage will increase as the distance increases. The test vessel has a length of 300mm, thus the sensor configuration can be seen in the plot below. One important thing to note is that the distance is for one length of the vessel (so it is half the total distance the sound pulses travel). This is following the same conventions followed by the sensor specification of the blind zone.

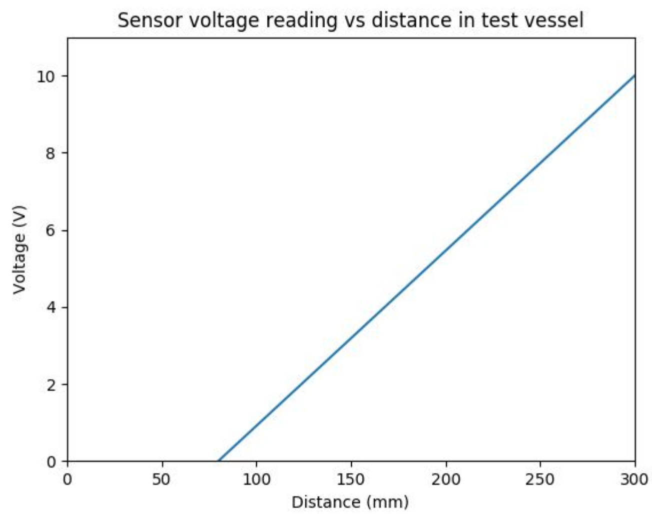

Figure 5: Sensor voltage variation with effective distance

The sensor has active temperature compensation, which means it will maintain 10V at the original set distance no matter the temperature. Meaning, that as the temperature changes, the voltage will not, i.e. the above plot is invariant to temperature.

Using this fact, the equation relating voltage to change in concentration can be obtained (see appendix C for detailed calculations and constants)

$$V = \Gamma\sqrt{\frac{Gx^2 + Hx + I}{Ax + B}} - Z \quad (2)$$

The active temperature compensation of the sensor causes this equation to be independent of temperature. Using equation 2, the following plot was created. Given a voltage reading the concentration of the mixture can be determined.

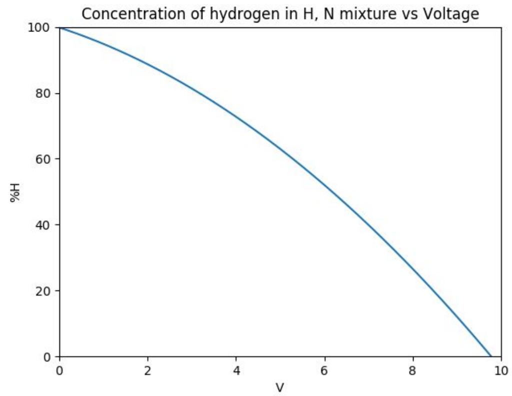

Figure 6a: Helium concentration variation with sensor voltage

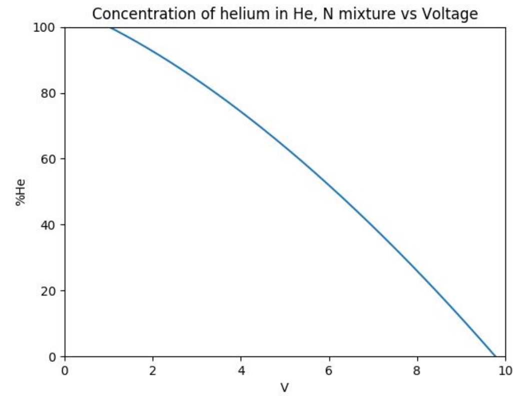

Figure 6b: Hydrogen concentration variation with sensor voltage

Another important consideration is the required minimum length of the vessel to stay out of the blind zone for 100% gas concentrations. For hydrogen this is 303.182mm, and for helium it is 234.983mm (appendix D). The vessel length used is 300mm long, thus it is sufficient for testing helium up to a 100% concentration, but it would be recommended to have a slightly longer vessel to test hydrogen if accurate measurements up to 100% hydrogen concentration were desired. This means that there would need to be a space of at least 303.182mm long within the anode of the fuel cell to implement this solution using this particular sensor. If detecting less than 100% concentration was sufficient then the minimum length would be shorter. This must be addressed when implementing this system within a fuel cell.

Sensitivity Analysis

In order to fully understand the dependencies within the system, a sensitivity analysis needs to be performed. For this project, it is measuring the effects of temperature, pressure and voltage output on the calculated gas concentrations.

From equation 2, the concentration is only a function of voltage and is independent of all other variables. This means it is not necessary to know the temperature or test chamber pressure to find concentration. However, for the purposes of a sensitivity analysis, these variables should be tested irregardless. This adds evidence to the assumptions that the gases behave ideally and that the concentration is truly invariant of temperature and pressure.

It is desired to be able to detect a $\pm 1\%$ change in concentration. The change in voltage versus percent concentration plots below were generated by taking the numerical derivatives of figures 6a and 6b. The largest magnitude of rate of change occurs in hydrogen at 100% concentration. This gives a maximum rate of change of $\Delta V_{max} = 23.2\Delta x$, which gives $\Delta V_{max} = 232mV$, for $\Delta x = 0.01$ (1%).

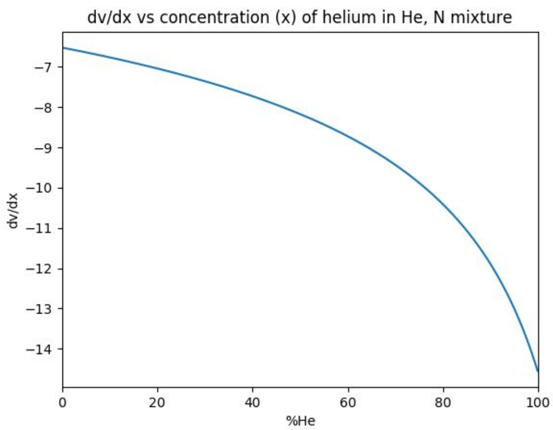

Figure 7a: Change in voltage per percent change in concentration as a function of concentration of helium

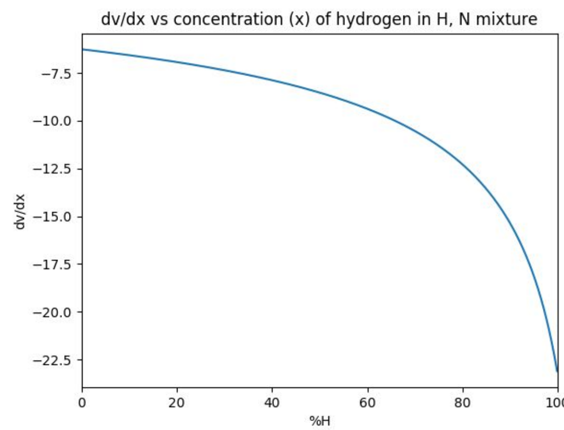

Figure 7b: Change in voltage per percent change in concentration as a function of concentration of hydrogen

An Stm32L432 microcontroller was used to read the voltage value from the sensor. This microcontroller has a 12bit analog to digital converter, and 3.3V tolerant analog input pins, which means it has a 0.806 mV resolution ($\frac{3.3V}{2^{12}}$). In order to get the sensor voltage reading down to a safe value for the analog inputs, a 3 to 1 voltage divider was used. This gives a minimum voltage change on the microcontroller pin of $(\Delta V_{max})_{controller} = 77mV$. In other words, a 1% change in hydrogen will cause a 77mV change in voltage on the analog pin, which is easily detected by the microcontroller (77mV > 0.807mV). The absolute error of the pin is four times the least significant bit, or 3.2mV, which is still significantly less than the calculated 77mV change.

Error Analysis

An error analysis was performed to determine the error bound on the % concentration from a voltage reading, the plots below were generated following the work in appendix E. Note that the maximum error occurs near low values of H_2/He concentration.

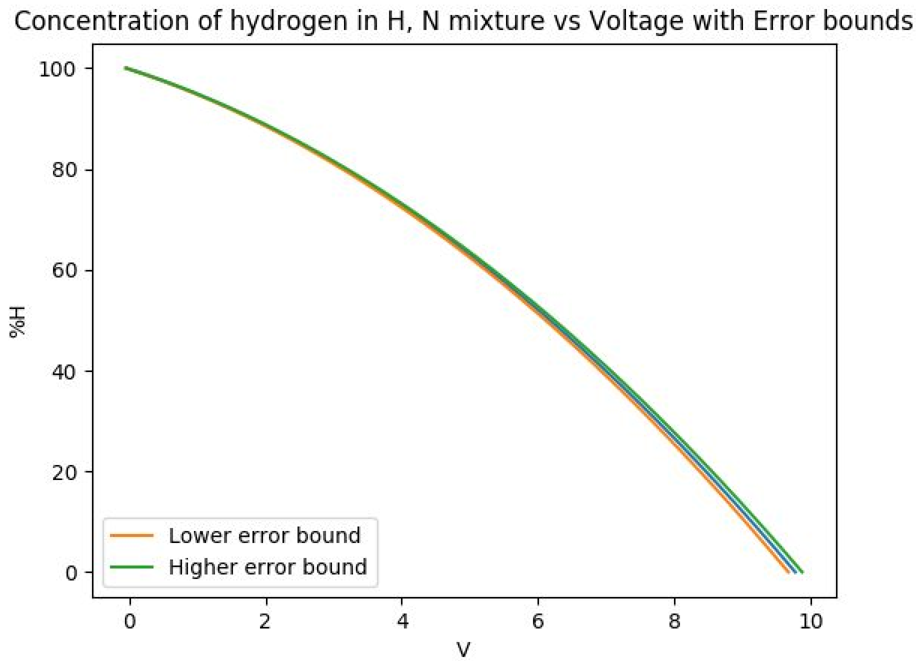
Concentration of hydrogen in H, N mixture vs Voltage with Error bounds
%H
V
Lower error bound
Higher error bound

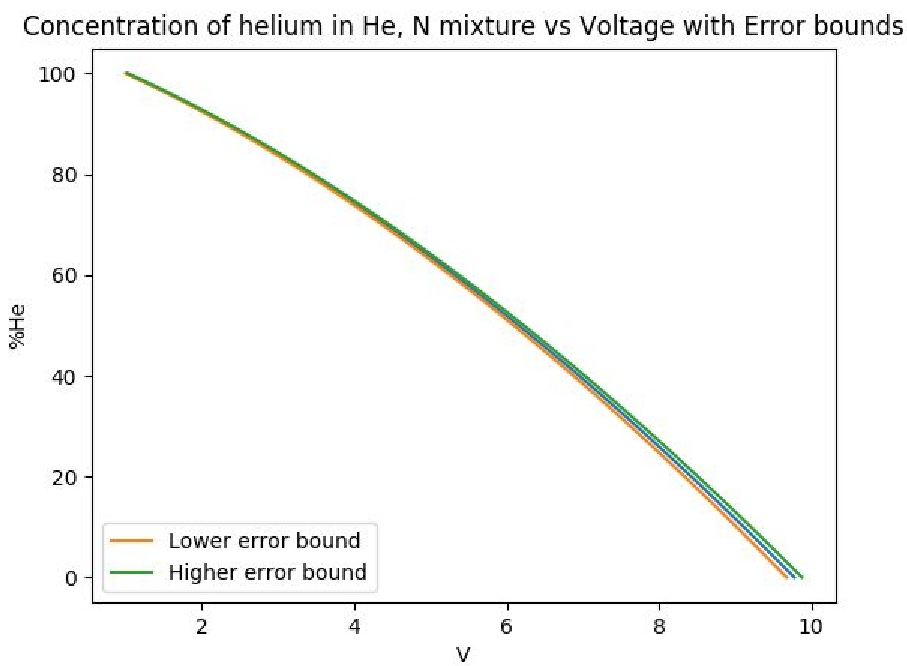
Concentration of helium in He, N mixture vs Voltage with Error bounds
%He
V
Lower error bound
Higher error bound

Design, approach, method, etc.

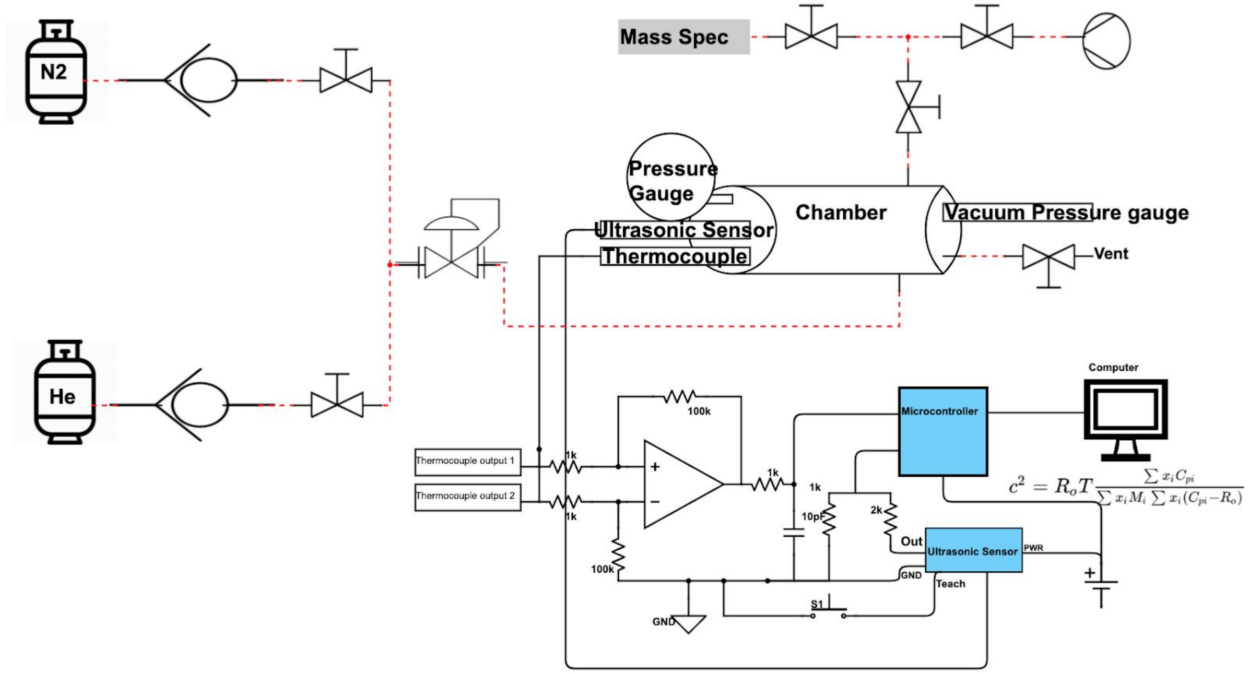

Figure 9: System level diagram (Electrical lines are black solid lines, pneumatic lines are red dashed)

In order to test the sensor's ability to detect small changes in the concentration, a testing chamber with nitrogen and helium inputs, one output (to the mass spectrometer), and various sensors were needed. OverdriveFCE provided a 300mm vacuum rated, stainless steel tube with removable end caps. This was ideal as it closely mimics the size and shape of the final location within a fuel cell vehicle. It also provided flexibility as the end caps could be modified so multiple sensor configurations could be tested. One of the caps was machined to fit a pressure gauge, thermocouple and the ultrasonic transducer. It was important to make sure the rod of the thermocouple did not interfere with the signal from the ultrasonic sensor. The thermocouples were positioned as far away (radially) as possible to minimize the risk of interference. The other instrumentation was positioned on the same side as the ultrasonic sensor in order to leave the other side of the chamber as flat as possible and maximize the reflected signal. The other cap was machined to fit a digital vacuum pressure gauge, as there was no space on the first cap, and it had no negative effect on the reflected signal. The cylinder already had 3 welded interfaces on the side that were used as a single gas input, an output for the mass spectrometer/vacuum line and a manual pressure release valve.

The thermocouple was connected to a 100 times differential amplifier and then to a low pass filter to eliminate small variations in the signal. This was then fed into an analog input of the microcontroller for data acquisition. This, combined with a reading from a thermometer near the microcontroller, gave accurate temperature measurements. The output from the ultrasonic sensor is wired to another analog input through a voltage divider. The signal was divided from 10V to 3.3V maximum so that the microcontroller can safely read it. The sensor was also wired to power and ground. The sensor can be calibrated to read different maximum distances through the teach input, and it was calibrated to read the length of the 300mm chamber as 10V.

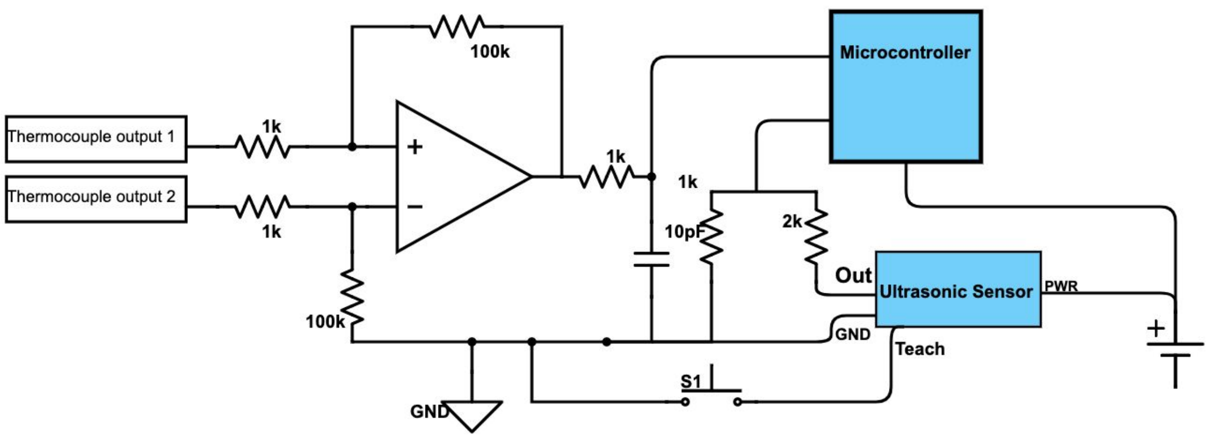

Figure 8: Circuit diagram for thermocouple and ultrasonic sensor

The gas chambers were connected through one-way and manual controlled valves, before the lines meet and flow through a pressure regulator into the chamber. This allowed for each gas to be flowed individually without any chance that it would contaminate the other line. One weakness was the barbed connections on the tank regulators that attached to the helium and nitrogen tanks. The plastic barbs are very fragile and it is difficult to get an adequate connection onto the hose that does not leak or blow off under pressure. It is our recommendation that these connections be replaced, if possible, with a better standard.

The output from the chamber into the mass spectrometer flowed through a manual control valve on the chamber side and into a 3 way junction. One of the connections was to the lab's vacuum system, which allowed for the system to be purged. The other connection is to a small leak valve which fed the mass spectrometer small amounts of the gas mixture.

All threaded interfaces were leak-proofed with teflon tape and tightened to the torque specified by the manufacturer. Tubing was connected with Swagelok® or equivalent fittings in order to ensure lasting, leak proof connections. Copper gaskets were used on the fittings within the mass spectrometer. A leak test was conducted by spraying helium over all of the joints of the system while it was under vacuum pressure and checking the mass spectrometer to see if any helium made its way into the system. The system had negligible leaks once all fittings were properly tightened.

Tests, results, and discussion of results

Due to COVID-19 shutdowns, we were unable to run the experiment and gather data. A test chamber was built which is capable of receiving two gas inputs, outputting a gas mixture to a mass spectrometer and reading pressure and temperature values. The chamber was verified to be leak proof. We were also able to informally see the expected variation in the voltage reading with changing concentrations by comparing to values read by the mass spectrometer. More work needs to be done to characterize and validate this observation.

Conclusions

The original objective was to prove that an acoustic sensor is able to determine the concentration of hydrogen within a gas mixture with ± 1% accuracy. The team observed that ultrasonic sensors are able to detect changes in the percentage of helium within a gas mixture. As the concentration of helium in the test chamber increased, the ultrasonic sensor output a decreased voltage to signify reading a decreased distance as sound travels faster as more hydrogen is introduced. By running further experiments, it would be possible to define a relationship between the voltage output from the ultrasonic sensor and concentration of helium (and therefore hydrogen) within a gas mixture. The ultrasonic sensor could then be applied within a fuel cell to monitor the hydrogen percentage and create a closed-loop control system as desired.

However, there are still some issues and concerns to be aware of when moving forward with the project. Currently, only a few, non-formal trials have been run so it is important to run more trials and to collect data before confirming that ultrasonic sensors are able to detect the concentration of hydrogen in a gas mixture with ± 1% accuracy. Furthermore, the experiments have only been run using gas mixtures of two gases, helium and nitrogen, so results may be different if gas mixtures consist of several gases and hydrogen is used in place of helium. Additionally, experiments have only been run at room temperature and the ability of ultrasonic sensors to accurately read the percent of hydrogen in a gas mixture may be affected with changes in temperature. Moreover, trials have only been run with a single ultrasonic sensor from ifm and the performance of other ultrasonic sensors may vary. Lastly, from the limited observations made by the team, there seems to be a delay between when the gas mixture concentrations are changed and when the ultrasonic sensor outputs a corrected voltage.

Recommendations

It is our recommendation to continue the project and move on to formal experimentation. Most changes will be in the form of quality of life improvements, however two larger changes are needed before exhaustive testing can be performed.

1. Perform a sensitivity analysis and ensure results are reproducible. Work needs to be done to investigate and characterize any small temperature and pressure dependencies of the system. Theoretically, for the sensor, there should be little interaction, but it is important to test that this is true and account for it if necessary.
2. Design of a temperature control system. For testing temperature extremes, a team would need to design a system to allow the chamber to reach thermal equilibrium. Since the sensor compensates for temperature, it is important that the sensor is at equilibrium to ensure that the read value is both stable and accurate.

The following are small improvements that can be added to the test chamber:

1. Attached a digital pressure gauge and emergency relief valve directly to the tank.
2. Change the barb-to-connect tank connectors to a more reliable connection. The barb connectors are useful for quick prototyping, but allow for trace amounts of contaminants to enter the system and prevent the test chamber from filling up to higher pressures.
3. Machine a seperate end cap that interfaces with different sensors.
4. Run the experiments with the Balluff sensor to see how measurements can vary with sensors.

Deliverables

1. Proposal
2. Testing Chamber
3. Sensors
4. Electrical and pneumatic circuits
5. Spare and unused parts
6. Contact information for Dr. Guillaume Bussiere (Appendix A)
7. Plot generation and data acquisition code:
   https://github.com/spennyp/accousticHydrogenSensor

Appendices

Appendix A: Technical Resources

Guillaume Bussiere

UBC Chemistry Department, Senior Instructor

Phone Number: 604-822-6384

Email: bussierg@chem.ubc.ca

Project Role: Expert in mass spectrometry, has available lab space to run experimental trials

Microcontroller Datasheet: https://www.st.com/resource/en/datasheet/stm32l432kc.pdf

Appendix B: Acoustic energy loss through medium boundaries

Ultrasound sensors work by propagating high frequency sound pulses through a medium, and then receiving those pulses on the other side of the medium or by reflecting the pulses off the medium boundary and receiving them where they were transmitted. Every medium has an acoustic impedance which is defined as $Z_{accoustic} = \rho * v$, where ρ is the medium density, and v is the speed of sound in that medium. The amount of reflected energy at the boundary between two mediums can then be defined in terms of these acoustic impedances[7]:

$$E_{Re} = (\frac{Z_2 - Z_1}{Z_2 + Z_1})^2$$

In the case of a hydrogen-aluminum boundary, 99.998% of the energy is reflected. In order for a non-intrusive system to work there would be at least two hydrogen-aluminum boundaries causing only 4×10^{-8}% of the original energy to be left over once the pulse reaches the receiver. With such a small amount of energy left at the receiver, the initial energy would need to be enormous to be detected.

Appendix C: Deriving Voltage in term of Composition

Equation 2 is derived in the derivation below using the fact the sensor has active temperature compensation.

$v = \frac{d}{t}$

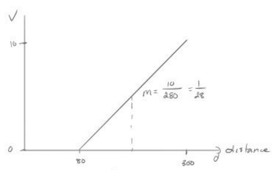

$\rightsquigarrow$ True for all T

$\Rightarrow$ holds true for all v of air as v changes w/ T

$$v_{air} = \sqrt{\frac{\gamma R T}{M}} = \sqrt{T}\,\frac{1}{\alpha}, \quad \alpha = \sqrt{\frac{M}{\gamma R}}, \text{ values for air}$$

$\Downarrow$

$$d = 22V + 80$$

$$t = \frac{d}{v}$$

$$\Rightarrow \quad t = \frac{22V + 80}{v} = (22V + 80)\frac{\alpha}{\sqrt{T}}$$

$\rightsquigarrow$ this tells us the general TOF given V, T

$v_{gas} = \frac{d}{t}$, $d = 300\text{mm}$ $\rightsquigarrow$ Not 600, since 80 blind zone accounts for single sided TOF

$$= \frac{300}{22V + 80}\,\frac{\sqrt{T}}{\alpha}$$

$\Rightarrow t$ is for TOF of one way

$$\text{Also, } v_g^2 = RT\,\frac{(xC_H + (1-x)C_N)}{(xM_H + (1-x)M_N)(x(C_H - R) + (1-x)(C_N - R))}$$

$\rightsquigarrow Ax + B$, $A = C_H - C_N$, $B = C_N$

$\rightsquigarrow (x(M_H - M_N) + M_N)(x(C_H - C_N) + C_N - R)$

$= (Cx + D)(Ex + F)$, $C = M_H - M_N$, $D = M_N$, $E = C_H - C_N$, $F = C_N -$

$= CE x^2 + x\underbrace{(CF + DE)} + DF$

$= Gx^2 + Hx + I$

$$v_g = \sqrt{RT}\sqrt{\frac{Ax + B}{Gx^2 + \quad I}}$$

$$\Rightarrow \sqrt{RT}\sqrt{\frac{Ax + B}{Gx^2 + Hx + I}} = \frac{300 \cdot 10^{-3}}{22V + 80}\,\frac{\sqrt{T}}{\alpha}$$

$$\Rightarrow \quad V = \left[\frac{300}{\sqrt{R}\,\alpha}\sqrt{\frac{Gx^2 + Hx + I}{Ax + B}} - 80\right]\frac{1}{22}$$

$$= \Gamma\sqrt{\frac{Gx^2 + Hx + I}{Ax + B}} - Z, \quad \Gamma = \frac{150}{11}\sqrt{\frac{\gamma}{M}}, \quad Z = \frac{40}{11}$$

It is also interesting to note the implications of active temperature compensation. Using the equations found in the derivation, the following plots were produced. One important thing here is that the voltage vs velocity plot is nonlinear, this is due to the fact that d is held constant, and voltage vs time of flight is linear so there is a 1/x relation for velocity.

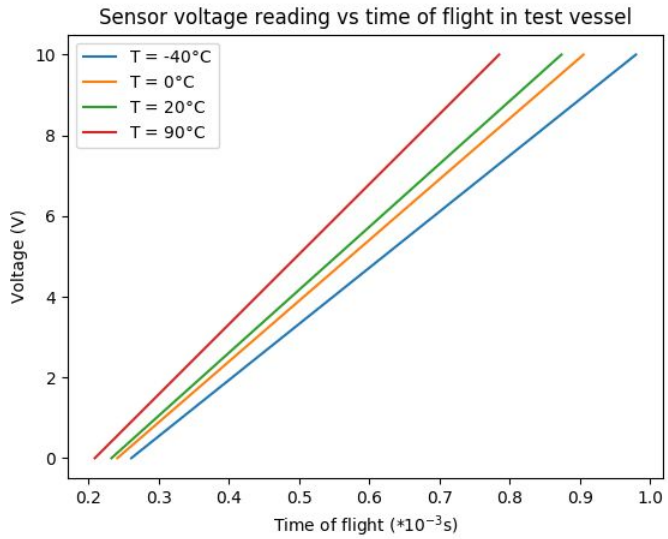
Sensor voltage reading vs time of flight in test vessel
T = -40°C
T = 0°C
T = 20°C
T = 90°C
Voltage (V)
Time of flight (*10^{-3}s)
0
2
4
6
8
10
0.2
0.3
0.4
0.5
0.6
0.7
0.8
0.9
1.0

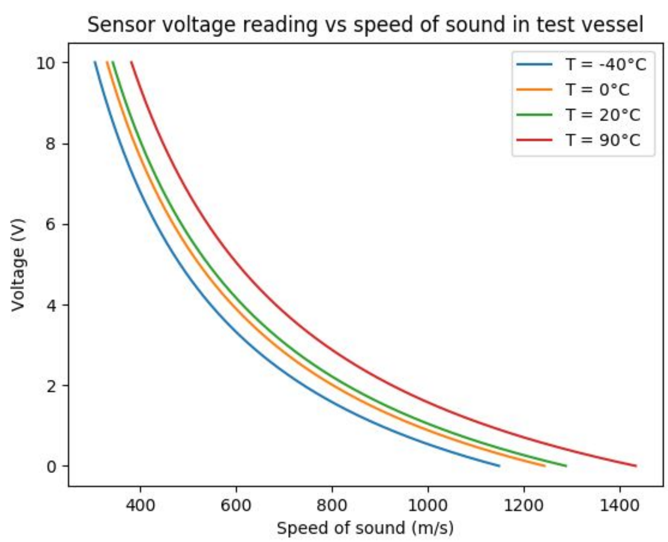
Sensor voltage reading vs speed of sound in test vessel
T = -40°C
T = 0°C
T = 20°C
T = 90°C
Voltage (V)
Speed of sound (m/s)
0
2
4
6
8
10
400
600
800
1000
1200
1400

Appendix D: Deriving Minimum Vessel Lengths

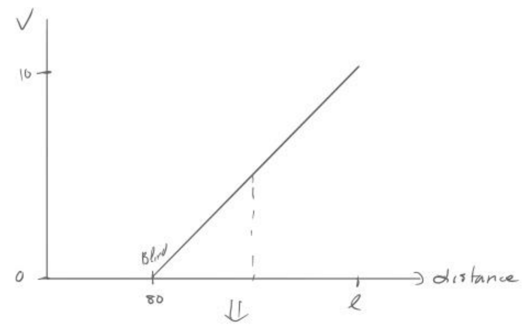

$$\Downarrow$$

$$d = \frac{l-80}{10} V + 80$$

$$t = \left(\left(\frac{l-80}{10}\right)V + 80\right)\frac{\alpha}{\sqrt{T}}, \quad \alpha = \sqrt{\frac{M}{\gamma R}} \text{ for air}$$

$$\nu = \frac{d}{t} \Rightarrow l = \left(\left(\frac{l-80}{10}\right)V + 80\right)\frac{\alpha}{\sqrt{T}}\,\nu, \quad \text{where } V = 0 \text{ (to find min } l\text{)}$$
$$\text{and } \nu = \sqrt{\frac{\gamma R T}{M}} \text{ for the gas}$$

$$\Rightarrow l_{min} = 80 \frac{\alpha}{\sqrt{T}} \sqrt{\frac{\gamma R T}{M}}$$
$$= 80 \sqrt{\frac{M_{air}}{\gamma_{air} R}} \sqrt{\frac{\gamma_{gas} R}{M_{gas}}}$$
$$= 80 \sqrt{\frac{M_{air}\gamma_{gas}}{M_{gas}\gamma_{air}}}$$

$$\boxed{\begin{aligned} (l_{min})_H &= 303.182 \text{ mm} \\ (l_{min})_{He} &= 234.983 \text{ mm} \end{aligned}}$$

Appendix E: Numerical Error Analysis

Taking the sensor error, and microcontroller error and equation for the min and max voltajes for a given actual voltage was found as follows.

Errors sensor output: < 1% → taking 1% for worst case

microcontroller input: LSB = 0.806 mV

- $4 \cdot LSB = 3.2\,mV$

$$V_{sensor} = V_{real} \overset{\text{sensor error}}{\pm V_{real} \cdot 0.01}$$

$$= V_{real}(1 \pm 0.01)$$

$$V_{controller} = (V_{controller})_{actual} \overset{\text{microcontroller error}}{\pm 3.2 \cdot 10^{-3}},$$

$$= \tfrac{1}{3} V_{real}(1 \pm 0.01) \pm 3.2 \cdot 10^{-3}$$

$$\Rightarrow \left.\begin{aligned} (V_{controller})_{max} &= 1.01\, V_{real} + 3.2 \cdot 10^{-3} \\ (V_{controller})_{min} &= 0.99\, V_{real} - 3.2 \cdot 10^{-3} \end{aligned}\right\} \text{Multiply by 3 in software, note resistor values introduce systematic error}$$

$\Rightarrow$ it can be corrected for w/ calibration

This was then used to plot the error curves alongside the voltage vs concentration curves to find the possible concentration error for a given voltage reading, which can be seen in the plots in the error analysis section.

Appendix F: Experimental Procedure

1. Connect the testing chamber to the mass spectrometer.
2. Close the leak valve to the mass spectrometer (MS) and the MS-to-chamber valve
3. Use vacuum to purge the system down to 1e-3 torr
4. Flow nitrogen into tank until it reaches atmospheric pressure
5. Close the purge valve and stop flowing nitrogen
6. Repeat steps 3-5 three times
7. Flow nitrogen into the system approximately to calculated pressure
8. Stop flowing nitrogen
9. Flow helium into system into tank to approximately higher calculated pressure
10. Wait for temperature to stabilize within 1°C for over a minute
11. Vacuum MS to chamber connection
12. Open the valve between the chamber and the MS
13. Flow and purge the connection 3 times
14. Slightly open the leak valve to MS until the pressure in the MS reaches 5e-6 torr
15. Use the MS software to get data on the gas composition
16. Read sensor voltage, pressure and thermocouple values
17. Use the sensor voltage to calculate the composition
18. Compare the calculated values to MS values

Appendix G: Bill of Materials

Date	Company	Order Number	Quantity	Part Number	Part Description	Cost Per Part	Total Cost
1/17/20	ifm	62199445	2	UGT508	Ultrasonic Diffuse Sensor	$216.00	$432.00
2/10/20	Balluff	73213996	2	BUS004T	Ultrasonic Sensor	$551.48	$1,102.96
2/19/20	McMaster	1458526	1	8520T4	SMC Air Regulator, Series AR30-B, 1/4 NPT Female	$49.10	$49.10
2/19/20	McMaster	1458526	2	3648K36	Quick-Connect Thermocouple Probe for Surfaces, Adhesive-Back, Type T	$66.17	$132.34
2/19/20	McMaster	1458526	2	6897K36	Micro M12 Signal/Power Connector, Straight Socket, 4 Pole, 1 Keyway, 12 Feet Cable	$39.96	$79.92
2/19/20	McMaster	1458526	2	6897K46	Micro M12 Signal/Power Connector, Straight Socket, 5 Poles, 1 Keyway, 12 Feet Cable	$49.74	$99.48
2/19/20	McMaster	1458526	1	5182K365	Yor-Lok Fitting for Stainless Steel Tubing, Straight Reducer for 3/8" x 1/4" Tube OD	$21.45	$21.45
2/19/20	McMaster	1458526	1	9262K986	Oil-Resistant Buna-N O-Ring, 2.7 mm Wide, 18 mm ID, packs of 25	$5.30	$5.30

2/19/20	McMaster	1458526	10	5182K326	Tube Support for 1/4" Tube OD Yor-Lok Fitting for Stainless Steel Tubing	$4.18	$41.80
2/19/20	McMaster	1458526	10	5182K111	Yor-Lok Fitting for Stainless Steel Tubing, Straight Adapter for 1/4" Tube OD x 1/4 NPT Male	$9.55	$95.50
2/19/20	McMaster	1458526	1	2525A173	Uncoated High-Speed Steel Pipe and Conduit Thread Tap, High-Speed Steel, Plug Chamfer, 1/4 NPT, 2-7/16" Overall Length	$24.94	$24.94
2/19/20	McMaster	1458526	1	4934A22	Thread Sealant Tape, 3M PTFE Model 547, 0.003" Thick, 1/4" Wide, 36 Yards Long	$12.78	$12.78
2/22/20	McMaster	1626300	2	7768K12	Brass Threaded Check Valve with Brass Spring-Loaded Piston, 1/4 NPT Female x NPT Female	$13.51	$27.02
2/22/20	McMaster	1626300	1	8520T4	SMC Air Regulator, Series AR30-B, 1/4 NPT Female	$49.10	$49.10
2/22/20	McMaster	1626300	2	8550T1	Joiner Clamp for SMC Compressed Air Frls for 1/4 and 3/8 NPT	$7.95	$15.90
2/22/20	McMaster	1626300	2	8562T1	Safety Lockout Valve for Compressed Air Frls, SMC Modular Series VHS30, 1/4 NPT Female	$39.36	$78.72
2/22/20	McMaster	1626300	3	33325K21	Corrosion-Resistant On/Off Valve, Lever Handle, Chrome-Plated Brass Body, 1/4 NPT Female x 1/4 NPT Female	$9.76	$29.28

2/22/20	McMaster	1626300	10	5182K111	Yor-Lok Fitting for Stainless Steel Tubing, Straight Adapter for 1/4" Tube OD x 1/4 NPT Male	$9.55	$95.50
2/22/20	McMaster	1626300	10	5182K326	Tube Support for 1/4" Tube OD Yor-Lok Fitting for Stainless Steel Tubing	$4.18	$41.80
2/24/20	McMaster	1686900	2	2384N12	Flow-Adjusting Valve for Gas Cylinder, CGA C10, 3/16" Tube ID Barbed	$108.33	$216.66
2/24/20	McMaster	1686900	1	5108K45	Abrasion-Resistant Polyurethane Tube for Air 3/16" ID, 1/4" OD, 25 ft. Length	$11.00	$11.00
2/24/20	McMaster	1686900	1	5548K75	Hard Nylon Plastic Tubing for Air and Water Semi-Clear White, 3/16" ID, 1/4" OD, 25 ft. Length	$12.50	$12.50
2/24/20	McMaster	1686900	1	3095A13	Multipurpose Cutter, 2-3/8" Cut Length	$26.78	$26.78
2/24/20	McMaster	1686900	1	5362K11	Worm-Drive Clamps with Thumb Screw for Firm Hose and Tube, 7/16" to 25/32" Clamp ID Range, packs of 5	$8.67	$8.67
2/24/20	McMaster	1686900	1	1520N22	Helium Gas, 3.7 cu. ft. Cylinder Capacity	$132.50	$132.50
2/24/20	McMaster	1686900	1	1520N42	Nitrogen Gas, 3.7 cu. ft. Cylinder Capacity	$132.50	$132.50

3/2/20	McMaster	2065110	1	1245N16	Threaded Thermocouple Probe for Liquids and Gases, Type T, 6" Long	$76.57	$76.57
3/2/20	McMaster	2065110	1	5113K31	Low-Temperature Firm EVA Plastic Tubing for Air & Water, Semi-Clear, 1/8" ID, 1/4" OD, 50 ft. Length	$10.50	$10.50
3/2/20	McMaster	2065110	1	80005K86	Nylon Cable Tie, Narrow, 3" Long, 8 lbs. Breaking Strength, Off-White, packs of 25	$5.73	$5.73
3/2/20	McMaster	2065110	1	8525K134	Electrical-Insulating Garolite XX Sheet, Brown, 12" x 24" x 1/4"	$23.56	$23.56
3/3/20	McMaster	N/A	2	5182K365	Yor-Lok Fitting for Stainless Steel Tubing, Straight Reducer for 3/8" x 1/4" Tube OD	$21.45	$42.90
3/3/20	McMaster	N/A	2	5182K506	Front and Back Sleeve for 3/8" Tube OD Yor-Lok Fitting for Stainless Steel Tubing	$7.07	$14.14
3/19/20	McMaster	2927738	1	2384N12	Flow-Adjusting Valve for Gas Cylinder, CGA C10, 3/16" Tube ID Barbed	$108.33	$108.33
Total							**$3,257.23**

Appendix H: User Manuals

UGT508

Ultrasonic sensor

UGB01200O2OG/US

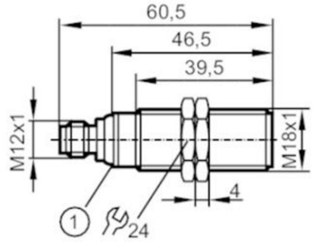

1 LEDs

Product characteristics		
Sensing range	[mm]	80...1200
Housing		Threaded type
Dimensions	[mm]	M18 x 1 / L = 60.5
Electrical data		
Operating voltage	[V]	10...30 DC; (cULus - Class 2 source required)
Current consumption	[mA]	< 35
Protection class		III
Reverse polarity protection		yes
Power-on delay time	[s]	0.1
Converter frequency	[kHz]	200
Inputs / outputs		
Number of inputs and outputs		Number of analog outputs: 1
Inputs		
Synchronization input		no
Multiplex input		no
Outputs		
Total number of outputs		1
Number of analog outputs		1
Analog voltage output	[V]	0...10
Min. load resistance	[Ω]	3000
Short-circuit protection		yes
Overload protection		yes
Monitoring range		
Sensing range	[mm]	80...1200
Blind zone	[mm]	80
Angle of aperture cylindrical	[°]	8; (±2)
Detection range hysteresis	[mm]	< 1
Max. deviation from the 90° angle sensor/object	[°]	± 4

UGT508

Ultrasonic sensor

UGB01200O2OG/US

Accuracy / deviations			
Temperature compensation		yes	
Hysteresis	[%]	< 1	
Switch-point drift	[%]	-2.5...2.5	
Linearity error of analog output	[%]	< 1	
Notes on the accuracy / deviation		The indicated values are reached after a warm-up time of min. 20 minutes	
Operating conditions			
Ambient temperature	[°C]	-20...70	
Protection		IP 67	
Tests / approvals			
EMC		EN 61000-4-2 ESD	4 kV CD / plastics
			8 kV AD / metal
		EN 61000-4-3 HF radiated	3 V/m
		EN 61000-4-4 Burst	2 kV
		EN 61000-4-6 HF conducted	3 V
		EN 55011	class A
Vibration resistance		EN 60068-2-6 Fc	(10-55) Hz 1 mm amplitude, vibration duration 5 min., 30 min. per axis with resonance or 55 Hz
Shock resistance		EN 60068-2-27 Ea	yes
MTTF	[years]	217	
Mechanical data			
Weight	[g]	79	
Housing		Threaded type	
Dimensions	[mm]	M18 x 1 / L = 60.5	
Thread designation		M18 x 1	
Material		stainless steel (1.4404 / 316L); PA; epoxy glass ceramics	
Displays / operating elements			
Display		Switching status	1 x LED, yellow
		echo	1 x LED, green
Accessories			
Accessories (supplied)		lock nuts: 2, stainless steel	
Remarks			
Remarks		cULus - Class 2 source required	
Pack quantity		1 pcs.	

Electrical connection

Connector: 1 x M12

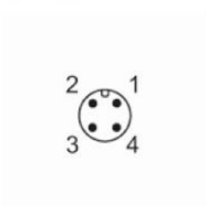

UGT508

Ultrasonic sensor

UGB01200O2OG/US

Connection

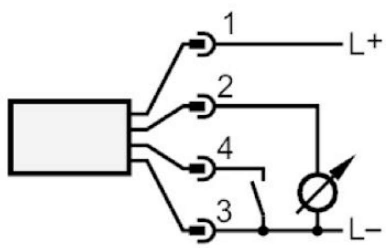

4: Teach

UGT508

Ultrasonic sensor

UGB01200O2OG/US

Diagrams and graphs

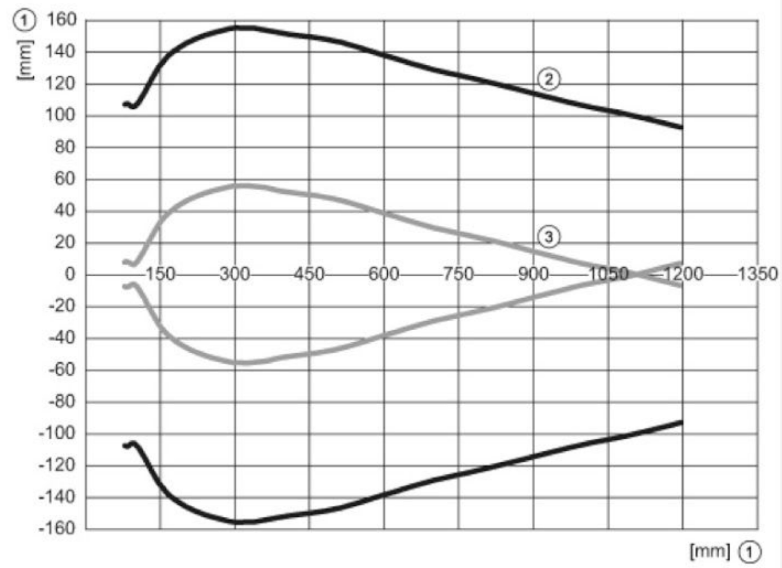

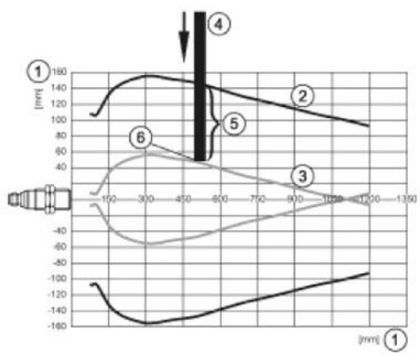

1: Distance

2: Monitoring range

3: switch-on/switch-off graph

4: Target 200 x 200 mm

5: 50 % of the target in the detection zone

6: Set point

Ultrasonic Sensors

BUS M18M1-XA-07/035-S92G
Order Code: BUS004T

BALLUFF

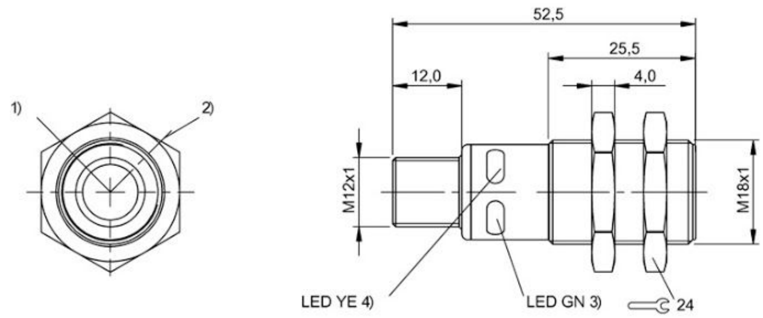

1) Ultrasonic transducer axis, 2) Exit direction 90° connector, 3) Operating voltage, 4) Output function

IND. CONT. EQ 5HP6 for use in the secondary of a class 2 source of supply

Display/Operation

Adjuster	no

Electrical connection

Connection	M12x1-Male, 5-pin
Polarity reversal protected	yes
Short-circuit protection	yes

Electrical data

Current draw max.	40 mA
Input function	Output curve rising/falling Teach in the working range Factory setting (Reset) Synchronization on/off Synchronization signal
Load resistance RL min. (Analog V)	100 kOhm at UB > 15 V
Operating voltage Ub	15...30 VDC
Rated operating voltage Ue DC	24 V
Synchronization	internal, max. 10 sensors
Ultrasonic Frequency	400 kHz

Environmental conditions

Ambient temperature	-25...70 °C
IP rating	IP67
Storage temperature	-40...85 °C

Functional safety

MTTF (40 °C)	1134 a

General data

Application	Distance measurement
Approval/Conformity	cULus LISTED CE EAC WEEE
Operating mode	Analog measurement (output curve)
Series	M18M1

Material

Housing material	Brass PBT
Material sensing surface	PU foam/Epoxy resin/Glass
Surface protection	nickel plated

Mechanical data

Dimension	Ø 18 x 52.5 mm
Mounting	Nut M18x1

Output/Interface

Analog output	Analog, voltage 0…10 V
Output characteristic	linear rising/falling

Range/Distance

Range	65...600 mm
Rated operating distance Sn	350 mm
Repeat accuracy	± 0.15 %FS
Resolution	≤ 0.069 mm

Connector Drawings

Wiring Diagrams

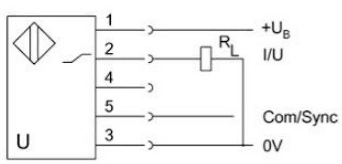

Technical Drawings

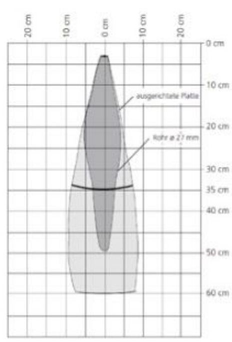

References

[1] C. F. Huang K. N.and Huang, Y. C. Li, and M. S. Young. “High precision, fast ultrasonic thermometer based on measurement of the speed of sound in air”. In: Review of Scientific Instruments 73.11 (2002), pp. 4022–4027. Url: https://doi.org/10.1063/1.1510576.

[2] R. Lueptow, S. Phillips, and M. Oczkowski. Acoustic Natural Gas Fuel Quality Sensor. Url: https://doi.org/10.4271/950529. (accessed: 11.10.2019).

[3] James Larminie and Andrew Dicks. “Fuel Cell Systems Explained”. In: John Wiley Sons Ltd, 2003. Chap. 1.

[4] Science Daily.Speed of sound. Url: https://www.sciencedaily.com/terms/speed_of_sound.htm. (accessed: 11.13.2019).

[5] Andrew Duffy. The gas laws. url: http://physics.bu.edu/~duffy/py105/Idealgas.html. (accessed: 11.13.2019).

[6] Torbjorn Lofqvist, Kestutis Sokas, and Jerker Delsing. Speed of Sound measurements in Gas-mixtures at Varying Composition Using an Ultrasonic Gas Flow Meter with Silicon Based Transducers. Url: https://pdfs.semanticscholar.org/30f6/64b5cdbc75ceb6fc34fe3c2079a04b401c88.pdf. (accessed: 10.10.2019).

[7] MIT. Specific Heats: the relation between temperature change and heat. Url: https://web.mit.edu/16.unified/www/FALL/thermodynamics/notes/node18.html. (accessed: 11.15.2019).

[8] Sakurambo.Solid oxide fuel cell. Url: https://commons.m.wikimedia.org/wiki/File:Solid_oxide_fuel_cell.svg. (accessed: 11.12.2019).

[9] Fernando Villanueva.Acoustic Impedance and Reflected Energy in Ultrasonics. Url: https://www.linkedin.com/pulse/acoustic-impedance-reflectivity-ultrasonics-fernando-villanueva/ .(accessed: 11.08.2019).16